LES OF COMLEX TURBULENT FLOWS WITH HIGH ORDER ACCURACY FINITE VOLUME METHOD

Guixiang Cui, Ruifeng Shi and Zhaoshun Zhang
Department of Engjneering Mechanics,
Tsinghua University
Beijing, China 100084
cgx@mail.tsinghua.edu.cn

Lan Xu
College of Science
Donghua University
Shanghai, China, 200051

ABSTRACT

The paper presents a high accuracy scheme for Finite Volume Method (FVM) with Immersed Boundary Method (IBM) with application to complex turbulent flows. Two testing cases are computed, namely flow passing three-dimensional hill and building arrays. The standard Smagroinsky model and Lagrangian dynamic model are used in LES for comparison in the case of flow passing building array. The results show that the proposed numerical method is capable of predicting complex flow with reasonable cost.

INTRODUCTION

Large eddy simulation is believed to be a potential prediction method for complex turbulent flows in foreseeable future (Piomelli, 1999), however, a number of problems are still needed to be further resolved before it can be used in practice. In addition to the physical issues, such as subgrid stress model and wall model etc., the accuracy and cost of computation are the major concerns in the practical development of LES for complex turbulent flows. The Pade finite volume compact method (Pereira et al. 2001) is used in LES of three dimensional unsteady flows in the paper. The higher order accuracy scheme can reduce the computational cost consierdably by use of coarse grids. Another problem in numerical method is to satisfy the non-slip condition at rigid wll with complex geometry. Although grid generation technique is available but the governing equation must be transferred to curvilinear coordintes. Multiblock grids should be generated if the geometrical configuration is very complicated. The situation is much worse in the coupling of moving boundary with stationary wall. The advantage of Immersed Boundary Method (IBM) is to solve the governing equations in Cartesian corrdinates with easy programming and less computational cost. An improvement of IBM accuracy is proposed and applied in the paper. As far as subgrid stress model is concerned the dynamic Smagorinsky model is robust and suitable for wall turbulence. In complex turbulent flow, however, there is no homogeneous direction which can be used in carrying out average in the dynamic procedure (Lilly, 1992), therefore the Lagrangian dynamic model (Meveneau, 1994) is used in the LES for complex turbulence flows. A backward facing step is computed for examining the higher order accuracy scheme and a flow passing 3D hill is computed successfully with immersed boundary method. The flow field and concentration distribution inside building array in the atmospheric boundary layer is simulated numerically by means of the proposed method with satisfaction.

NUMERICAL METHOD

The governing equation

The governing equations of large eddy simulation can be written as:

$$\frac{\partial(\rho\bar{u}_i)}{\partial x_i}=0 \tag{1}$$

$$\frac{\partial(\rho\bar{u}_i)}{\partial t}+\frac{\partial(\rho\bar{u}_i\bar{u}_j)}{\partial x_j}=-\frac{\partial\bar{p}}{\partial x_i}+\mu\frac{\partial^2\bar{u}_i}{\partial x_j\partial x_j}+\frac{\partial(\rho\tau_{ij})}{\partial x_j} \tag{2}$$

$$\frac{\partial(\bar{\theta})}{\partial t}+\frac{\partial(\bar{\theta}\bar{u}_j)}{\partial x_j}=\kappa\frac{\partial^2\bar{\theta}}{\partial x_j\partial x_j}+\frac{\partial T_j}{\partial x_j} \tag{3}$$

in which τ_{ij} and T_j are the subgrid stress and thermal flux respectively with eddy model as follows

$$\tau_{ij}=2\nu_t\bar{S}_{ij}+\frac{1}{3}\tau_{kk}\delta_{ij},\ \ \nu_t=C\Delta^2\left|\bar{S}\right| \tag{4}$$

$$T_j=k_t\frac{\partial\bar{\theta}}{\partial x_j},\ \ \kappa_t=\frac{\nu_t}{Pr_t} \tag{5}$$

in which ν_t, κ_t are the subgrid eddy viscosity and eddy diffusivity, respectively with turbulent Prandtl number $Pr_t=$ 0.70. Both simple Smagorinsky model and dynamic model are tested for comparison with C_s = 0.1 for Smagorinsky model. For Lagrange dynamical model proposed by Meveneau (1996) the model coefficient $C = I_{LM}/I_{MM}$

$$\frac{\partial I_{LM}}{\partial t}+\bar{u}_j\frac{\partial I_{LM}}{\partial x_j}=\frac{1}{T}\left(L_{ij}M_{ij}-I_{LM}\right) \tag{6}$$

$$\frac{\partial I_{MM}}{\partial t}+\bar{u}_j\frac{\partial I_{MM}}{\partial x_j}=\frac{1}{T}\left(M_{ij}M_{ij}-I_{MM}\right) \quad (7)$$

in which $T=1.5\Delta\left(I_{LM}I_{MM}\right)^{-1/8}$

The fourth order accuracy FVM

The fourth order accuracy FVM is formulated by Padé type compact interpolation of flow variables between the centre of the elements and centers of element surfaces. The stencil of the FVM is shown in Figure 1 and one dimensional fourth order Padé type compact scheme for interior points in *x* direction can be written as follows

$$a_i\tau_{h_i}\bar{\phi}^{yz}+\bar{\phi}^{yz}+b_i\tau_{-h_i}\bar{\phi}^{yz}=c_i\tau_{h_i/2}\bar{\phi}^{xyz}+d_i\tau_{-h_i/2}\bar{\phi}^{xyz}+O(h^4) \quad (8)$$

in which $h_i=x_{i+1}-x_i (i=1,2,\cdots,N-1)$ are mesh lengths of the grids and

$$a_i=h_{i-1}^2/(h_i+h_{i-1})^2 \quad (9a)$$

$$b_i=h_i^2/(h_i+h_{i-1})^2 \quad (9b)$$

$$c_i=2(h_{i-1}+2h_i)h_{i-1}^2/(h_i+h_{i-1})^3 \quad (9c)$$

$$d_i=2(h_i+2h_{i-1})h_i^2/(h_i+h_{i-1})^3 \quad (9d)$$

and $\tau_{\Delta x}$ is a shift operator defined as $\tau_s f(x)=f(x-s)$. In equation (8) $\bar{\phi}^{xyz}$ is the volume average of ϕ at center of the element and $\bar{\phi}^{yz}$ is the average of ϕ on the element surfaces. Similar formula can be derived for the boundary points and the derivatives of ϕ. The full details of the fourth order accuracy formulation for three dimensional flow, including for the non-uniform grid, can be found elsewhere (Xu, 2005).

The improvement of IBM

In IBM an external force is added to N-S equation near the rigid boundary that

$$\frac{\partial(\rho\bar{u}_i)}{\partial t}+\frac{\partial(\rho\bar{u}_i\bar{u}_j)}{\partial x_j}=-\frac{\partial\bar{p}}{\partial x_i}+\mu\frac{\partial^2\bar{u}_i}{\partial x_j\partial x_j}-\frac{\partial(\rho\tau_{ij})}{\partial x_j}+f_i \quad (10)$$

in which the force term is given by

$$f_i=-RHS+\frac{V_{bi}-u_i^n}{\Delta t} \quad (11)$$

The term RHS contains the pressure gradient, advection and diffusion terms and V_{bi} is the velocity of the rigid wall if the grid point coincides with the rigid wall. The solution of equation (8) and (9) satisfies exactly the non-slip condition at the wall. However it is almost impossible and one has to use interpolation between wall and interior grids to obtain V_{bi} at the nearest grid points to the wall. The accuracy of IBM depends on the interpolation scheme and lower order interpolation, e.g. linear interpolation, reduces the accuracy of the numerical solution of LES. A third order spline interpolation is used in the proposed FVM and the improvement of numerical prediction will be shown later in the testing case in comparison with the linear interpolation.

The fourth order Runge-Kutta integration is used in the time advancement of the LES.

RESULTS

The flow over back-facing step

The flow Reynolds number equals 5100 (U_0H/ν), in which U_0 is free stream speed and *H* is the height of the step.

The computational domain is a rectangular box with streamwise length of 30*H*, spanwise width of 4*H* and normal height of 6*H*. The inlet velocity condition is posed by the data of fully developed turbulent channel flow. Periodic condition is posed in spanwise direction and non-reflection condition is posed at outlet and upper boundary. Wall function with power law (Werner and Wengle 1991) is used at the rigid wall and dynamic Smagorinsky model for the subgrid stress. Uniform grids are used in spanwise direction while non-uniform grids are prescribed in normal and streamwise directions near rigid walls, the total grids are $172\times83\times32$ in streamwise, normal and spanwise directions respectively. The statistics are taken average over time and spanwise direction. The results are compared with the DNS by Hung et al (1997) with grid points $768\times192\times64$.

The mean streamlines are shown in Figure 2 and the mean reattachment length is calculated and equal to 6.43*H*, which is in good agreement with DNS result of 6.28*H.* **F**igure 3 presents the comparison of statistical properties between LES and DNS at *x/h*=6. The example indicates the feasibility of the present numerical scheme to the separating and reattching flow.

The flow passing 3d hill

Flow around a three-dimensional hill is a typical case for examining numerical method. The Reynolds numbers equals 13000 based on the height of hill *H* and free stream velocity U_∞. The size of computational domain is $16H\times3.2H\times12H$ in streamwise, normal and spanise directions respectively. The Cartesian coordinates are used with grid numbers of $101\times84\times86$. The boundary conditions are similar to the backward facing step case with exception at the wall where the IBM method is used for satisfying non-slip condition.

The mean velocity field behind the hill is shown in Figure 4 and the profile of turbulent kinetic energy is shown in Figure 5(a) at *X*/*H*=3.63, *Z*/*H*=0.4886. Figure 5(b) demonstrates the mean pressure distributions at the hill surface. In Figure 4 and 5 the comparison with previous computational results by RANS model (Wang et al. 2004) is presented together with the experimental measurements (Byun, 2005). All predicted results by proposed method show good agreement with experimental measurements and better than RANS model.

The flow passing building array

An array of cubic buildings is studied with height *H*, length *B* and width *W* of 0.12m as shown in Figure 6. The flow Reynolds number based on the free stream velocity and the height of the building is equal to 4×10^6. The flow domain and non-uniform grids are illustrated in Figure 7. A point source is located at 10W in front of the building array.

The boundary conditions are posed as follows. At the inlet the mean streamwise velocity is given by a logarithm profile plus random velocity fluctuations with Gaussian probability density. Non-reflection condition is posed at outlet and fully developing condition at lateral boundaries, i.e.

$$\frac{\partial \overline{u}_i}{\partial t} + \overline{u}_1 \frac{\partial \overline{u}_i}{\partial x_1} = 0 \text{ , at } x/B\text{=70} \quad (12)$$

$$\frac{\partial \overline{u}_i}{\partial x_2} = 0 \text{ , at } y/B\text{=0 and } y/B\text{=30} \quad (13)$$

The mirror condition is given at upper boundary

$$\frac{\partial \overline{u}_1}{\partial x_3} = \frac{\partial \overline{u}_2}{\partial x_3} = 0 \text{ and } \overline{u}_3 = 0 \text{ at } z/b\text{=10} \quad (14)$$

The mean velocity profile inside building array is shown in Figure 9 with the experimental measurements by Davidson (1996) with fairly good agreement. The spanwise averaged mean velocity and concentration are demonstrated in Figure 10 and 11 respectively. The results show that the Lagrangian dynamic model is much better than standard Smagorinsky model although the later gives qualitatively reasonable results. Figure 12 demonstrates the flow pattern inside building array. It clearly shows separating zones behind building. In this case the individual building is similar to an isolated roughness. Figure 13 shows the effect of wind field on the concentration distribution that the higher wind speed the lower concentration. When the wind speed is over 2m/s its influence on the concentration is negligible.

DISCUSSIONS AND CONCLUDING

As mentioned before the accuracy of interpolation in IBM is important for the numerical accuracy of LES. The above numerical results of 3D hill are computed by the third order spline interpolation in IBM. For comparison the results computed by linear interpolation in IBM are presented in Figure 14 together with those by third order spline interpolation. It clearly shows the improvement of numerical results by use of higher order interpolation in IBM.

In the prediction of local wind field inside building array, which is similar to the residence area, the inlet turbulence intensity in the atmosphere is an important parameter. There are various ways to impose inlet boundary condition for turbulent boundary layer (Lund, 1998), however it is difficult to use recycling method in the complex turbulent flow. A simple addition of the inlet velocity fluctuations with sufficient inlet length is used in this paper and it is acceptable for the flow passing building array as shown in Figure 15 in which the numerical prediction of turbulent kinetic energy is in good agreement with experimental results while the turbulent kinetic energy can not be generated without inlet turbulence intensity.

In summary the proposed numerical scheme is capable of predicting complex turbulent flows with inclusion of the higher order interpolation in IBM, inlet turbulence intensity and Lagrangian dynamic model.

ACKNOWLEGEMENT

The authors would like to thank National Natural Science Foundation of China (NSFC Grant 10572073).

REFERENCES

Byun G. 2005 “Structure of three-dimensional separated flow on symmetric bumps“ PhD Thesis, Virginia Polytechnic Institute and State University. 2005

Davidson M.J. et al. 1996 “Wind tunnel simulation of plume dispersion through groups of obstacles“ Atmospheric Environment. **30**(22):3715-3731

Hanna S.R. et al. 2002 “Comparisons of model simulations with observations of mean flow and turbulence within simple obstacle arrays“ Atmospheric Environment 36: 5067-5079.

Hung L. and Moin P., Kim J. 1997 “Direct numerical simulation of turbulent flow over a backward-facing step“ Journal of Fluid Mechanics 330:349–374

Lilly D.K. 1992. “A proposed modification of the Germano subgrid-scale closure method” Physics of Fluids**,** A4:633

Lund T. 1998 Generation of turbulent inflow data for spatially-developing boundary layer simulation. Journal of Computational Physics 140**:**233-258

Pereira J. M. C., Kobayashi M H and Pereira I C F. 2001 “A fourth-order-accurate finite volume compact method for the incompressible Navier-Stokes solution“ Journal of Computation Physics; 167: 217－243.

Meneveau C. et al. 1996. “A Lagrangian dynamic subgrid-scale model of turbulence“ JFM, 319:385

Piomelli U. 1999 “Large-eddy simulation: achievements and challenges“ Prog. Aerosp. Sci.; 35: 335-362

Wang C. and Jang Y.J. and Leschziner M.A. 2004 “Modelling two- and three-dimensional separation from curved surfaces with anisotropy-resolving turbulence closures“ International Journal of Heat and Fluid Flow 25:499-512

Werner H, and Wengle H. 1991 “Large-eddy simulation of turbulent flow over and around a cube in a plate channel“ The Eighth International Symposium on Turbulent Shear Flows. Berlin: Springer-Verlag, 1941-1946

Xu L. 2005 “Study on high accurate finite volume method for large eddy simulation and its application to Reversible Runner“ Doctorial dissertation Thesis Tsinghua University

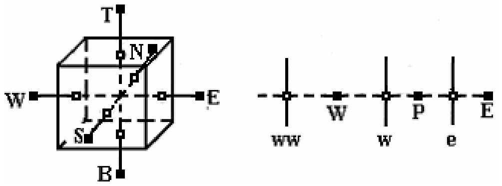

Figure 1 The stencil of FVM

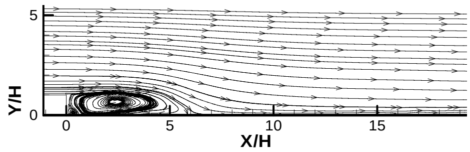

Figure 2 The mean streamline over back-facing step

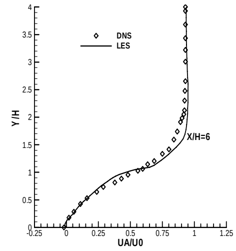

(a)

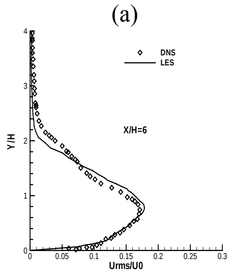

(b)

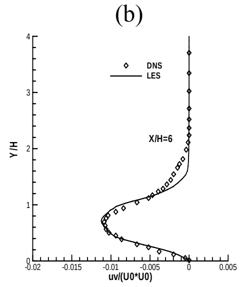

(c)

Figure 3 The statistics of turbulent flow over back-facing step. (a) The mean velocity profile, (b) The turbulent kinetic energy, (c) Reynolds stress

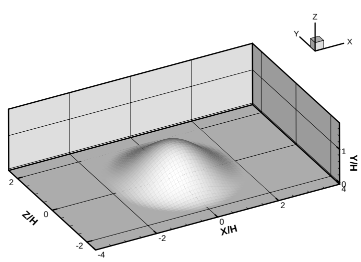

Figure 4 The configuration of 3-D hill

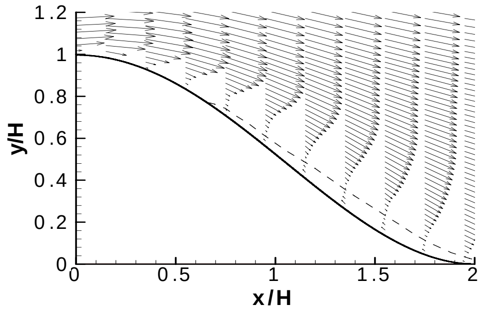

(a)

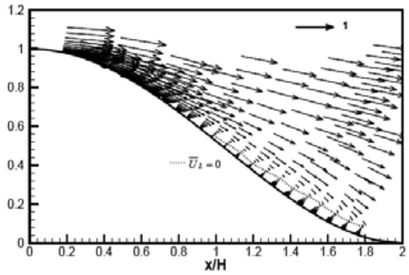

(b)

Figure 5 The mean velocity over 3-D hill
(a) Computed by present method,
(b) measurement by Byun (2005)

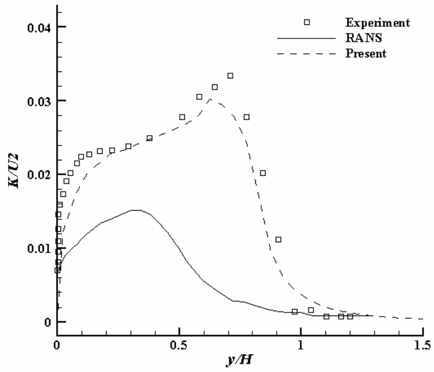

(a)

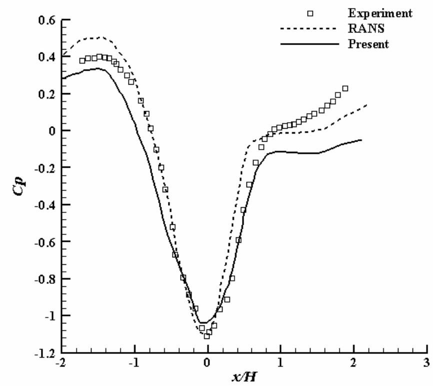

(b)

Figure 6 The statistics of turbulent flow over 3D hill
(a) The turbulent kinetic energy
(b) The pressure distribution

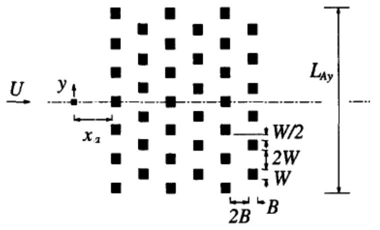

(a)

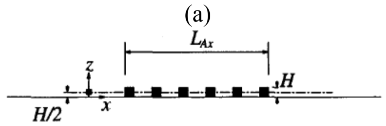

(b)

Figure 7 The configuration of building array
(a) top view, (b) side view

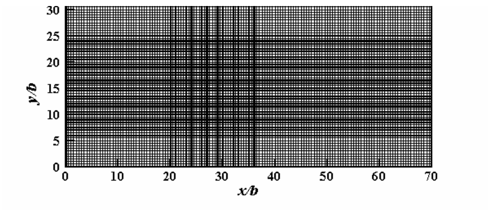

(a)

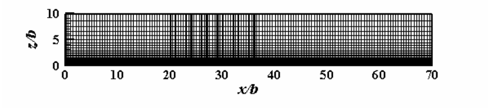

(b)

Figure 8 The grid for building array
(a) top view, (b) side view

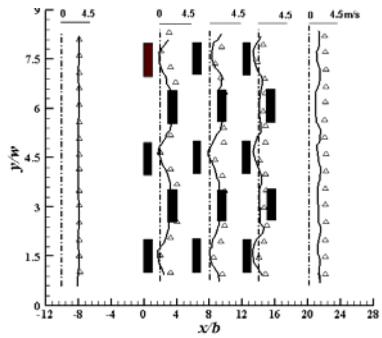

(a)

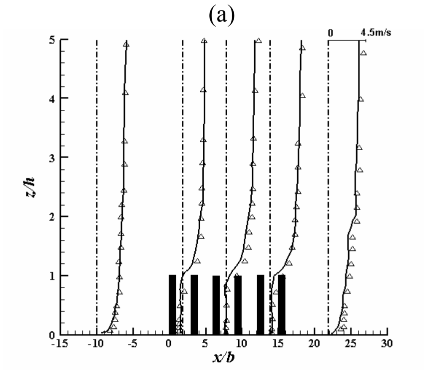

(b)

Figure 9 Mean velocity profiles in the building array
(a) Spanwise profiles, (b)Vertical profile

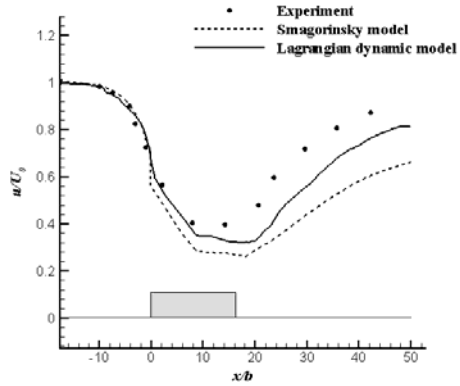

Figure 10 The spanwise averaged mean veolcity

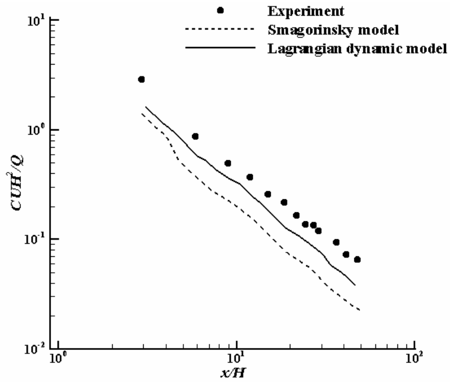

Figure 11 The spanwise averaged mean concentration

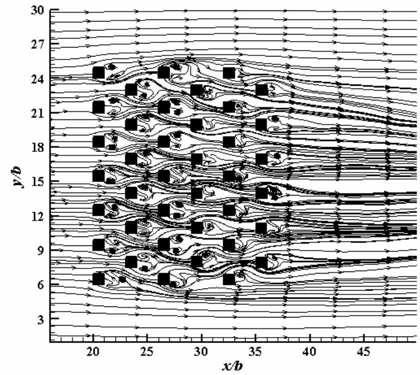

(a)

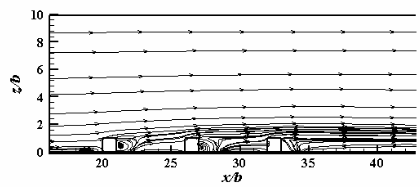

(b)

Figure 12 Flow patterns inside building array

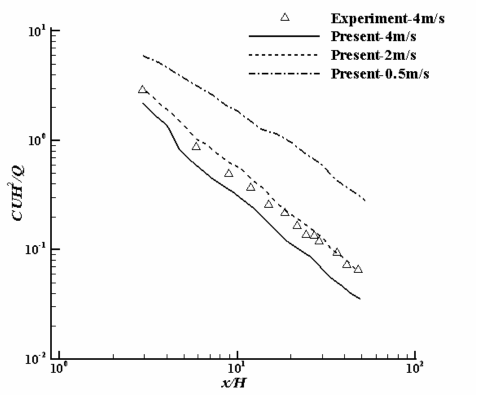

Figure 13 Effect wind spees on the concentration

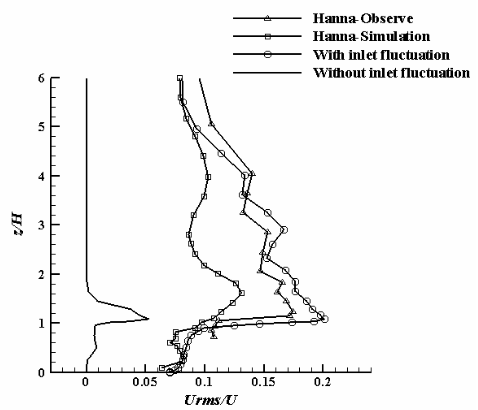

Figure 14 Influence of inlet turbulence intensity on the numerical result of turbulent kinetic energy

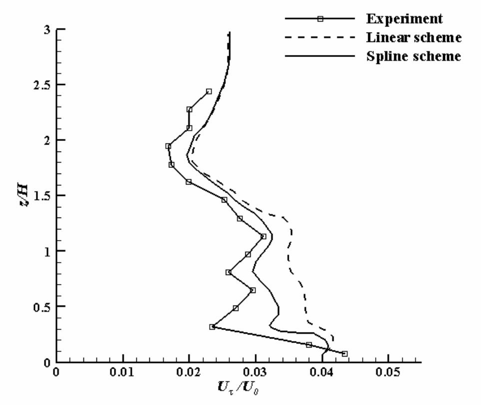

Figure 15 Comparison of the prediction accuracy between linear and third order spline interpolation in IBM